Toxicity of Luminescent Silica Nanoparticles to Living Cells

ARTICLE *in* CHEMICAL RESEARCH IN TOXICOLOGY · SEPTEMBER 2007

Impact Factor: 3.53 · DOI: 10.1021/tx7001959 · Source: PubMed

4 AUTHORS, INCLUDING:

Yuhui Jin
University of Washington Seattle
26 PUBLICATIONS **1,170** CITATIONS
SEE PROFILE

Min Wu
University of North Dakota
118 PUBLICATIONS **1,773** CITATIONS
SEE PROFILE

Toxicity of Luminescent Silica Nanoparticles to Living Cells

Yuhui Jin,[†] Shibichakravarthy Kannan,[‡] Min Wu,*[,‡] and Julia Xiaojun Zhao*[,†]

Department of Chemistry and Department of Biochemistry and Molecular Biology, University of North Dakota, Grand Forks, North Dakota 58202

Received March 31, 2007

Luminescent nanomaterials can provide high-intensity and photostable luminescent signals when used as labeling materials for the determination of trace amounts of analytes. However, a major concern that has arisen is whether the nanomaterials cause toxic effects in living systems. Here, we address this problem through a systematic investigation of the cytotoxicity and genotoxicity of luminescent silica nanoparticles. These nanoparticles are intensely luminescent labeling materials for ultrasensitive determination of biological samples. The investigation of genotoxicity of the nanomaterials was carried out from two perspectives. First, the integrity of the DNA was examined by detecting DNA base modification, strand breaks, and increased DNA repair activity to recover the damage. Second, different sets of cellular DNAs, including nuclear DNA extracts and the whole genomic DNAs, were examined. Furthermore, to fully assess DNA damage by the nanoparticles, isolated genomic DNAs were directly exposed to the nanoparticles. The cytotoxicity of the nanoparticle was detected by measuring the cell proliferation rate, cell death, and death patterns (necrosis and apoptosis) after the nanoparticle treatments. Results show no significant toxic effects due to the luminescent nanoparticles at the molecular and cellular levels below a concentration of 0.1 mg/mL. Our study indicates that the luminescent silica nanoparticle is a promising labeling reagent for various biomedical applications.

Introduction

Nanotechnology, in combination with biomedical developments, offers the promise of revolutionary tools for biomedical analysis (*1*). One of the most promising applications of such a combination is the application of highly luminescent nanomaterials as tags for identification and quantitation of small amounts of biological targets. To date, several important luminescent nanomaterials, including quantum dots (QDs) [1] (*2–5*), probe encapsulated by biologically localized embedding (PEBBLEs) (*6, 7*), liposomes (*8, 9*), and dye-doped nanoparticles (*10–14*), have been developed as luminescent tags for these purposes. However, the question of whether these nanomaterials are toxic to living cells or organisms has not been fully answered. Before promoting further applications of these nanomaterials in the biomedical field, systematic toxicological characterizations of the luminescent nanomaterials in living systems are critically needed.

Among different types of luminescent nanomaterials, QDs are the most popular due to their unique fluorescence properties—emitting long lifetime, narrow band width, fluorescence signals whose wavelengths vary as the size of QDs varies. The dye-doped silica nanoparticle is also a very attractive luminescent nanomaterial because it is doped with thousands of dye molecules in a single nanoparticle and thus gives a strong fluorescence signal. Toxicological characterization of the luminescent nanomaterials has been initiated by investigating the toxicity of QDs (*15–19*). The first toxicity study on Cd QDs was reported by Derfus and co-workers (*18*). Currently, the most widely used QDs are made from cadmium and selenium. Severe cytotoxic effects of cadmium selenide (CdSe) QDs were observed even at a relatively low concentration of the QDs (*15–19*). The extent of cytotoxic effects was correlated with the concentration of the released Cd^{2+}. Initial research indicates that the release of Cd^{2+} ions from CdSe QDs after surface oxidation is a key reason for the cytotoxicity (*18*). In contrast to the toxicity study of QDs, there are few similar investigations of luminescent silica nanoparticles. Therefore, the primary focus of this work is to systematically characterize the toxicological behavior of the luminescent silica nanoparticles in living systems. In addition, preliminary toxicity studies on QDs have focused on assessing the cellular toxicity of QDs. To our best knowledge, there are no reports of systematic studies of genome damage by nanomaterials. In this work, we have employed state-of-the-art techniques to investigate the genotoxicity of luminescent silica nanoparticles.

Several different dye-doped luminescent silica nanoparticles have been developed using the reverse microemulsion method (*11, 20*). Thousands of dye molecules are incorporated into a single nanoparticle during the formation of the silica nanoparticle by polymerization of tetraethylorthosilicate. Such a large number of dye molecules in a single nanoparticle provides a strong luminescence signal. By conjugating molecular recognition reagents to the nanoparticle surface, the nanoparticles have demonstrated an excellent signaling capability for the ultrasensitive determination of trace amounts of biological targets (*10–14*). For instance, using conjugates of antibody nanoparticles as luminescent tags, a single target bacterium was identified from a mixture of bacterial cells by fluorescence measurement and without pre-enrichments (*14*). In this work, to verify whether

* To whom correspondence should be addressed. Tel: 701-777-3610. Fax: 701-777-2331. E-mail: (M.W.) minwu@medicine.nodak.edu or (J.X.Z.) jzhao@chem.und.edu.

[†] Department of Chemistry.

[‡] Department of Biochemistry and Molecular Biology.

[1] Abbreviations: CdSe, cadmium selenide; DMEM, Dulbecco's modified Eagle's medium; MTT, 3-(4,5-dimethylthiazol-2-yl)-2,5-diphenyltetrazolium bromide; NBS, newborn bovine serum; PEBBLEs, probe encapsulated by biologically localized embedding; PFGE, pulse field gel electrophoresis; QDs, quantum dots; RuBpy, tris(2,2′-bipyridyl)dichlororuthenium(II) hexahydrate; TMR, tetramethylrhodamine.

10.1021/tx7001959 CCC: $37.00
Published on Web 07/13/2007

different types of dye molecule-doped nanoparticles are different in toxicity, both organic and inorganic dye-doped silica nanoparticles have been studied. Two typical dye molecules were chosen, tetramethylrhodamine (TMR) and tris(2,2′-bipyridyl)-dichlororuthenium(II) hexahydrate (RuBpy). TMR has been used as a labeling reagent in bioanalysis for years (*21*), and RuBpy is a common inorganic dye molecule (*12, 13*).

The luminescent silica nanoparticles have two principle components: porous network-structured SiO_2 and incorporated dye molecules. Unlike Cd QDs that are made from toxic heavy metal ions, these two components in the silica nanoparticles have less individual toxicity, although silica accumulation over a long term may induce chronic toxicity (*22*). Thus, it is expected that the luminescent silica nanoparticles may have low toxic effects. However, as molecules/atoms are made into nanometer-sized units, some properties of the nanomaterials are clearly different from their bulk materials, such as optical, mechanical, and electrical properties (*23*). So far, it is unclear whether molecules/atoms exhibit significant changes in their toxicological behavior when they are engineered to nanoscopic dimensions.

In this study, we investigated the potential toxicity of luminescent silica nanoparticles in cultured cells for up to 3 days. Studies involved testing for DNA base modifications, DNA strand breaks, whole genome toxicity, DNA repair protein responses, necrosis, and apoptosis.

Materials and Methods

Chemicals. TMR and RuBpy were purchased from ICN Biomedicals Inc. Acetic acid, polyoxyethylene(10) isoooctylphenylether [triton X-100,4-(C_8H_{17})C_6H_4(OCH_2CH_3)$_{10}$-OH], and tetraethylorthosilicate were purchased from Aldrich Chemical Co. Inc. (Milwaukee, WI). Cyclohexane, *n*-hexanol, acetone, and ammonium hydroxide (28–30%) were obtained from Fisher Scientific Co. (Pittsburgh, PA). TMR and RuBpy dye-doped luminescent silica nanoparticles were not commercially available. The nanoparticles were synthesized using a reverse microemulsion method (*11–13, 20*). The size of nanoparticles was 50 ± 3 nm in diameter. The obtained silica nanoparticles were resuspended in PBS solution with 0.02% sodium azide for long-term storage. MUA-QDs (the carboxyl-coated QDs) were purchased from Nanomaterials & Nanofabrication Laboratories.

Incubation of Cells with the Nanoparticles. The human lung epithelial cells (A549, purchased from ATCC, Manassas, VA) were used for the in vitro study of the nanoparticle toxicology. At day one, 1.0×10^6 cells were placed in each well of a six-well plate in 900 μL of Dulbecco's modified Eagle's medium (DMEM) containing 10% newborn bovine serum (NBS, purchased from Hyclone) and cultured for 24 h at 37 °C. The next day, 100 μL of the nanoparticle in pH 7.0 PBS buffer was added to the cell culture plate for the incubation. The final concentrations of nanoparticles ranged from 1×10^{-4} to 0.50 mg/mL (equivalent to 10^8 to 5×10^{11} nanoparticles/mL). The incubation time was different according to the designed experiments. The cells were collected after certain time periods for the toxic effect tests. The negative control cells were treated with DMEM containing 100 μL of PBS. The positive control cells were prepared differently based on the requirements of each individual assay. During all of these treatments, the cells were incubated at 37 °C in a 5% CO_2 and humidified atmosphere.

Penetration of the Nanoparticles into Mammalian Cells. About 5000 lung epithelial A549 cells were first cultured in DMEM containing 10% NBS for 24 h at 37 °C in a MatTek glass-bottom microwell dish (MatTek Corp., Ashland, MA). The cells were gently washed by pH 7.4 PBS buffer three times, incubated in 100 μL of pH 7.4 PBS buffer in a 37 °C chamber for confocal imaging, and directly observed under a Carl Zeiss LSM 510 Meta laser scanning confocal microscope (Carl Zeiss MicroImaging, Inc, Thornwood, NY). The fluorescence images were taken using a 63× objective lens with an excitation wavelength of 488 nm and a 585 nm long pass emission filter. Then, PBS-buffered RuBpy dye-doped silica nanoparticles were added to the culture dish at a final concentration of 0.50 mg/mL. The same setting for parameters was used for both controls and nanoparticles throughout the process. For the 3 day experiments, cells were incubated with 0.50 mg/mL of RuBpy dye-doped silica nanoparticles for 3 days and fluorescence images were taken after three washes with PBS buffer to reduce background signals. The experiments with alveolar macrophages were performed using the same procedures. Alveolar macrophages were isolated from Sprague–Dawley rats (Charles River Laboratories) using our previously published methods (*38*), and animal work was performed in accordance with the IACUC guidelines (approved by the UND IACUC committee).

Comet Assay. A549 cells (about 1×10^6 cells/well in a six-well plate) were incubated with different concentrations of the nanoparticles for certain time periods. Then, both the control cells and the nanoparticle-treated cells were washed and resuspended in Ca^{2+}- and Mg^{2+}-free PBS solution. The cell suspension was mixed with liquefied agarose at a ratio of 1:10 (v/v). A small aliquot of this mixture was immediately transferred onto the slide from Trevigen (comet assay kit). After cell lysis at 4 °C, slides were treated with alkali solution (0.3 M NaOH and 1 mM EDTA) for 60 min to unwind the double-stranded DNA. Slides were electrophoresed at 1 V/cm for 10 min and then stained with SYBR green dye after which they were observed under a confocal microscope (Carl Zeiss MicroImaging, Inc.). The comet tail length was defined as the distance between the leading edge of the nucleus and the end of the tail. At least 75 determinations were performed for each sample using CometScore software.

Pulse Field Gel Electrophoresis (PFGE). According to Elia's procedure (*24*), after they were incubated with nanoparticles, the cells were suspended into 1% buffered agarose and cast in plastic molds. The molds were incubated in a lysis buffer (TE buffer with 1% SDS and 0.30 mg/mL proteinase K) overnight at 37 °C. Prior to electrophoresis, the sample molds were washed several times with a pH 7.5 buffer containing 10 mM Tris-HCl and 1 mM EDTA. The MJ Research PPI-200 programmable controller was used for running gel electrophoresis overnight using program 8 at 180 V of applied voltage.

Western Blot Analysis of DNA Adducts. The improved Western blot method was employed as described in ref *25*. Nuclear extracts were essentially isolated using the reported method (*26*). Briefly, A549 cells were lysed in a hypotonic buffer at 4 °C for 30 min and then centrifuged at 4000 rpm for 10 min. The pellet was resuspended in HEPES buffer for 1 h following centrifugation at 12000 rpm for 10 min. These samples and the marker were subjected to SDS–PAGE electrophoresis (10%) at a constant voltage of 100 V for 2 h. The gel was then electroblotted to presoaked immobilon-P membrane (Millipore) at a constant current of 35 mA over 12 h in a transfer buffer (192 mM glycine, 20 mM Tris-HCl, and 10% methanol). The membrane was blocked by 5% dry milk for 2 h at room temperature. Then, the membrane was incubated with the first antibody (anti-8-oxo-dG mouse monoclonal antibody, clone IF7, Trevigen) at a dilution of 1:1000 at room temperature for 2 h. The membrane was briefly rinsed with deionized water and washed with TBS-T (50 mM Tris-HCl, pH 7.5, 150 mM NaCl, and 0.5% Tween-20) three times for 10 min per wash. The 1:2000 dilution of secondary horseradish peroxidase-conjugated anti-mouse antibody was then added to react with the membrane at room temperature for 2 h. Finally, the membrane was signaled by a luminescent reagent and was exposed on the Lumi-Imager. Using the image analysis software (Boehringer Mannheim Biochemicals, Germany), the band intensities were analyzed using the densitometry software. An equal loading was confirmed by staining the gel with the Coomassie blue dye.

DNA Agarose Gel. The genomic DNA from A549 cells was isolated using TRIzol reagent from Invitrogen (Carlsbad, CA) following the manufacturer's instructions. The purified DNA solution was diluted to 6.53 μg/mL with a TE buffer and measured

by a gene quant spectrophotometer (Amersham, Piscataway, NJ). The DNA solution was incubated with the luminescent silica nanoparticles for 2–3 days. Then, the molecular marker and the samples were run in a 0.8% agarose gel at 30 V and 15 mA for 6 h in TAE buffer. The gel was exposed under UV light, and the images were recorded using a camera.

DNA Repair Enzyme Activity Assay. The hOgg1 enzymatic activity was detected by the cleavage of a 23 bp oligonucleotide substrate containing a single 8-oxoguanine lesion (5′-GAA-CTA-GTG-**O**-ATC-CCC-CGG-GCT-GC-3′, Trevigen, Gaithersburg, MD). Cell lysates from nanoparticle-treated cells were reacted with 0.10 pmol of γ^{32}P-dATP end-labeled 23 bp DNA substrate at 37 °C for 1 h in 100 μL of analysis buffer [10 mM *N*-(2-hydroxyethyl)piperazine-*N*′-2-ethanesulfuric acid-KOH, pH 7.4, 10 mM KCl, 10 mM EDTA, and 0.10 mg/mL bovine serum albumin]. The reaction was terminated by the addition of 90% formamide loading buffer. After denaturing polyacrylamide gel (20%) electrophoresis, the DNA species were separated. The gel was dried and exposed on an X-ray film. The fractions of full DNA length and separated substrate were determined through densitometric analysis using the Kodak analysis software. The APE1 activity was detected using a 20 bp oligonucleotide (CCT-GCC-CTG-**THF**-GCA-GCT-GTG-GG, Trevigen) with the same method for hOgg1 enzymatic activity detection as described above. A control of cell lysates without nanoparticles during the cell culture was analyzed as well. The positive control cells were treated with 100 μM Cd^{2+} solution for 4 h.

Cell Proliferation Assay [3-(4,5-Dimethylthiazol-2-yl)-2,5-diphenyltetrazolium Bromide Assay]. A549 cells were mixed with different concentrations of nanoparticles in a 96-well plate. To avoid interferences between the nanoparticles and the tetrazolium salt of a detection reagent from a cell titer 96 nonradioactive cell proliferation assay kit (Promega, Madison, WI), the nanoparticles used were pure silica nanoparticles containing no fluorescent dye molecules. A premixed optimized dye solution was added to the plate wells, and then, the cells were incubated at 37 °C for 4 h. In this period, the living cells converted the tetrazolium component of the dye solution into a formazan product that showed absorption at 570 nm in a UV–vis spectrum. The formazan product was solubilized, and the absorbance at 570 nm was measured using a 96-well plate reader.

Trypan Blue Exclusion Assay. To measure the cell suspension percentage that is viable, Trypan Blue dye was employed to stain the cells that do not have intact membrane. The viable cells exclude the dyes and are not stained, which is a standard method to detect cell death. First, A549 cells were cultured with silica nanoparticles doped with different dyes or QDs in a 96-well plate. Then, the cells were dissociated from the bottom of the plate by trypsin. Finally, 10 μL of the Trypan Blue dye was added to each well. The viable cell amount was counted through a hemacytometer, and the viability values were derived by comparing the samples with the negative control.

Vybrant Apoptosis Assay. Cell apoptosis was detected by the Vybrant apoptosis assay. A549 cells were grown in a cell culture medium containing pure silica nanoparticles for 2–3 days. Afterwards, the cells were treated with the fluorescent probe propidium iodide and YO-PRO-1 dyes (Vybrant apoptosis assay kit, Molecular Probe, Eugene, OR) over 5 min. Before they were loaded on slides, the cells were washed with PBS buffer to remove the extra dye molecules. The slides were observed under a Zeiss confocal fluorescence microscope immediately. Living cells showed no fluorescent signals while apoptotic cells were stained by the green YO-PRO-1 dye.

Results and Discussion

Penetration of the Nanoparticles into Cells. Prior to investigating the cytotoxicity of the luminescent silica nanoparticles, we need to understand the interaction of the nanoparticles with the cells during the cell proliferation. The fact of whether the nanoparticles could be actively taken into cells would significantly affect their cytotoxicity. If the nanoparticles remain outside the cells, the toxicity would be minimal. Therefore, we first investigated the nanoparticle penetration during the cell culture. The lung epithelial A549 cells were incubated in a cell culture medium containing 0.50 mg/mL of RuBpy dye-doped silica nanoparticles using a MatTek glass-bottom microwell dish (MatTek Corp.) within a 37 °C chamber. The fluorescence images were taken using a Zeiss laser scanning confocal fluorescence microscope. As shown in Figure 1, at the beginning, the nanoparticles were dispersed around cells in the medium. As the incubation time increased, the nanoparticles penetrated into the cells and showed concentrated fluorescence signals on the inside of the cells. In general, the nanoparticles can be completely taken into A549 cells within 6 h and remain in the cells for up to 72 h. From the images, we have also observed an important fact that no fluorescent signals were present in the cell nuclear position, indicating that the nanoparticles remained outside the cell nuclei.

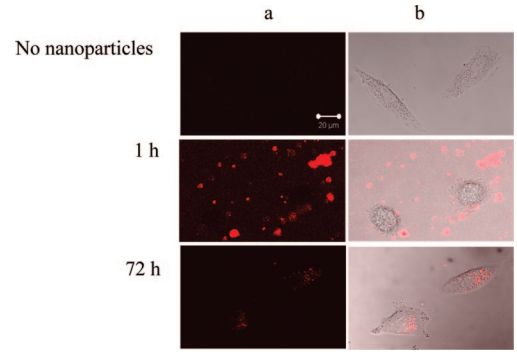

Figure 1. Penetration of the luminescent nanoparticles into A549 cells. (a) Fluorescence image. (b) Merge image of fluorescence and bright field images. Objective, 63×; excitation wavelength, 488 nm; and emission filter, 580 nm long pass filter. The samples were placed in a chamber slide in a bath at 37 °C.

The ability of the nanoparticle penetrating into cells varies upon cell types. Macrophages are a remarkable example for rapidly taking in nanoparticles due to their exceptional ability to phagocytose extracellular particles. We examined internalization rates of the luminescent nanoparticles into freshly isolated alveolar macrophage cells from female Sprague–Dawley rats (Harlan, Indianapolis, IN). The nanoparticles rapidly entered cells within 5 min of incubation. After 30 min, the amount of nanoparticles that entered the cells reached the maximum. As compared to the A549 cells, the nanoparticle penetration rate was much faster in the rat alveolar macrophages.

To further verify that the nanoparticles indeed penetrated into the cells and were not stuck on the cell surface, we scanned and reconstructed three-dimensional (3D) images to view various sections of the cells using a confocal fluorescence microscope (Figure 2). The internalized nanoparticles were confirmed by performing a Z series of confocal images. Surface-adherent particles can be easily distinguished from internalized nanoparticles by 3D reconstruction of the Z series using the Zeiss LSM software. The fluorescence intensity was observed in the section of the cell center, indicating that the nanoparticles entered the cells. However, there is no indication that the nanoparticles entered into the nucleus of the cell, consistent with the observation below that the nanoparticles did not cause significant genotoxicity.

In the following experiments, both TMR- and RuBpy-doped luminescent silica nanoparticles were employed. The two nanoparticles showed the same extent regarding the toxicity to living cells. The figures shown here were all based on RuBpy-doped silica nanoparticles.

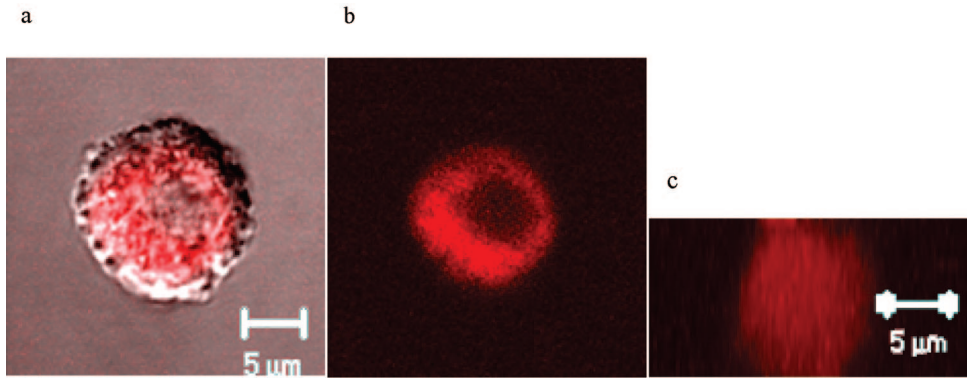

Figure 2. Nanoparticles location in the cells by imaging a cell at different Z sections. The fluorescence in the central section indicates that nanoparticles penetrated into the cell. (a) Merge of fluorescence and bright field images. (b) Fluorescence image. (c) Fluorescence image of the central section of the cell.

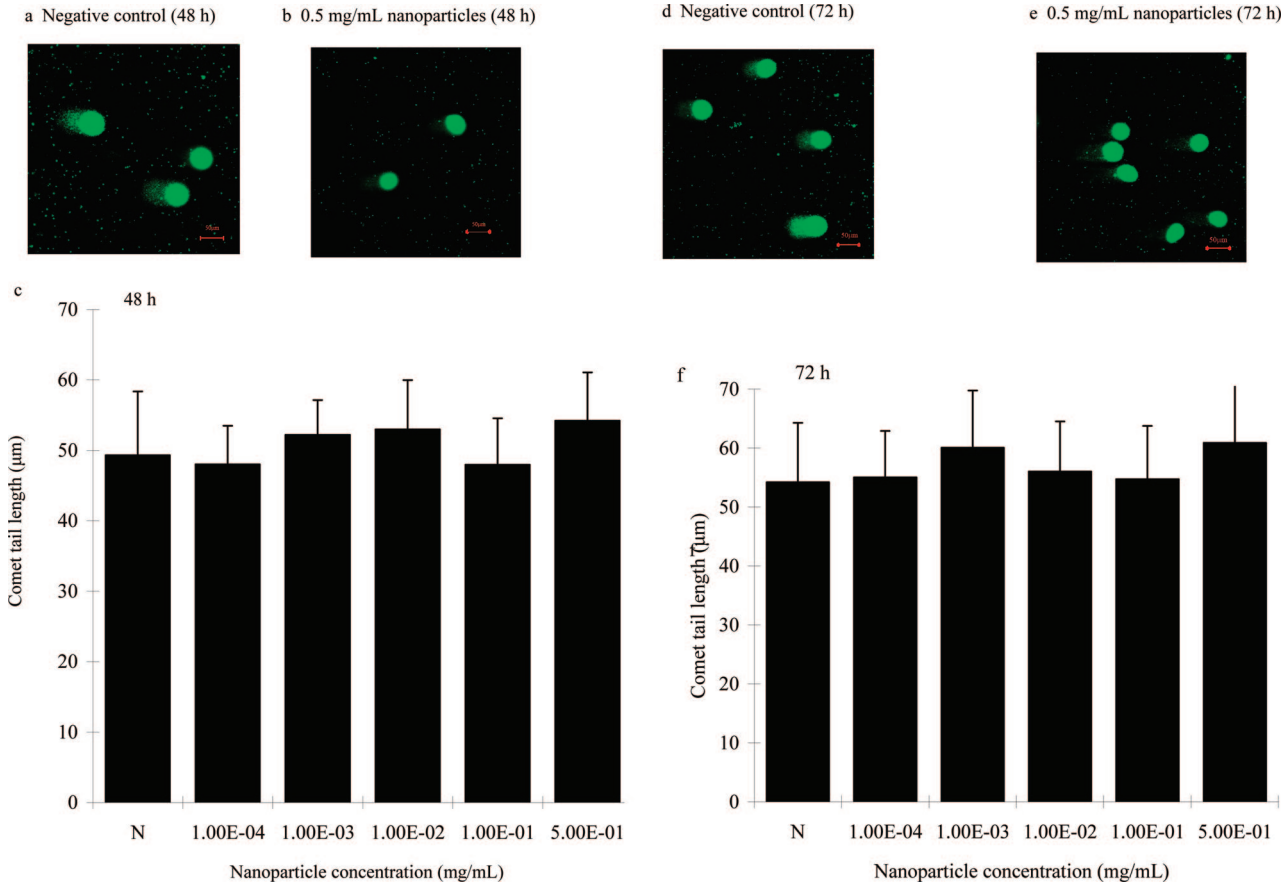

Figure 3. Detection of DNA strand breaks by the comet assay. (a) Representative fluorescence image of the negative control human lung A549 cells following 48 h of incubation with a medium containing PBS. (b) Representative fluorescence image of the luminescent silica nanoparticle-treated A549 cells following 48 h of incubation at the indicated concentrations. (c) Column graph showing the average tail lengths after being incubated with different concentrations of the luminescent silica nanoparticles for 48 h. Data are shown with means ± SD. (d) Fluorescence image of the negative control A549 cells for 72 h of incubation. (e) Fluorescence image of the cells treated with 0.5 mg/mL of the luminescent silica nanoparticles. (f) Column graph showing the average cell tail lengths after being incubated with different concentrations of the luminescent silica nanoparticles for 48 h. Data are shown with means ± SD (at least 75 cell comet tails were counted in each sample). All data are representative of more than three experiments.

Study of DNA Damage Induced by the Nanoparticles. We first examined the nanoparticle toxicity at the molecular level, that is, whether it would induce DNA damage in living cells. The integrity of DNA sequences is essential for maintaining genetic stability. DNA damage is associated with apoptosis, tissue injury, and carcinogenesis (*27, 28*). To comprehensively understand whether the nanoparticles can damage DNA in living cells, examinations were carried out using multiple approaches described as below.

Investigation of DNA Single Strand Breaks. DNA single-strand breaks were first investigated using whole cells as targets based on a comet assay. The A549 cells were incubated with the nanoparticles as described in the Materials and Methods. If any DNA single strands were broken, the cell would produce a comet tail on the fluorescence images. The comet tail length is considered proportional to the amount of DNA damage experienced by the cell. Because of the normal series of cell treatments in the comet assay, some artificial DNA lesions

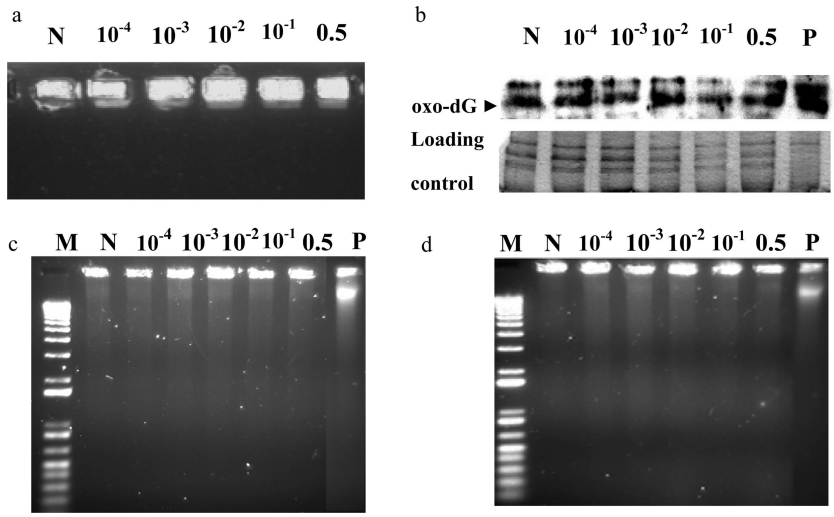

Figure 4. Investigation of potential DNA damage caused by the luminescent silica nanoparticles. The nanoparticle concentrations are 1.00×10^{-4}, 1.00×10^{-3}, 1.00×10^{-2}, 1.00×10^{-1}, and 0.50 mg/mL. N, negative control (PBS only); P, positive control (1 mM cadmium for 4 h); and M, 1 kbp DNA ladder. (a) PFGE of the whole genomic DNA from the nanoparticle-treated A549 cells. The cells (10^6/well in a six-well plate) were incubated with the nanoparticles for 72 h. An equal amount of prepared cell samples (in agarose molds, see the Materials and Methods) was loaded to a PFGE gel, and the gel was electrophoresed overnight. (b) Western blot analysis for the detection of DNA oxidative adducts in A549 cells by oxo-dG antibodies. Equal loading was confirmed by Coomassie Blue stain of the gel. (c and d) Analysis of damage to isolated genomic DNA by the nanoparticles using 0.8% agarose gel. The genomic DNA was isolated from A549 cells using Trizol reagents, and the DNA (2 μg/sample) was directly incubated with the nanoparticles in TE buffer at 37 °C in a dark room at room temperature for 48 (c) and 72 h (d).

always occurred. As shown in the negative control after treatment with PBS for 48 h, the average tail length was 49.3 $\pm$ 9.1 μm (Figure 3a). While the tail lengths of samples treated with different concentrations of nanoparticles ranged from 48.0 $\pm$ 6.6 to 54.2 $\pm$ 6.8 μm, these were not significantly different from the control (Figure 3b,c, $P > 0.05$, analyzed by Student's *t* test). When the nanoparticle treatment time was increased to 72 h (Figure 3d–f), results showed a slight increase in DNA single-strand breaks as compared to that of the 48 h tests ($P > 0.05$). The results suggest that the nanoparticles do not cause a significant number of DNA strand breaks.

The comet assay result was further verified using PFGE. Unlike the comet assay, the PFGE assay directly analyzes genomic DNA integrity at the whole cell level without additional manipulation. If the sample contains significant DNA lesions in chromosome structures, it will migrate faster than the control in a PFGE electrophoresis. After they were incubated with the nanoparticles for 72 h, the cells were directly assessed using PFGE analysis (Figure 4a). Each sample showed one clear band at the same position as the negative control, indicating no additional DNA damage as compared to the untreated control.

Study of DNA Base Modification. We next examined whether the nanoparticles could induce DNA base modification. The nuclear extracts were isolated from the nanoparticle-treated cell lysates for the determination of 7,8-dihydro-oxodeoxyguanine (oxo-dG), a common DNA lesion in a single base. Previously, oxo-dG was determined using Western blotting, which demonstrated compatible results to the traditional ECD-HPLC method, but specificity was enhanced (*29*). Here, we used an improved Western blot method (*25*). The positive control showed two intense dark bands against the negative control, indicating a significant increase in oxo-dG. The nuclear extracts from nanoparticle-treated cells demonstrated similar band densities to the negative control (Figure 4b, $P > 0.05$), suggesting that no significant increase in oxo-dG was induced in the cell nuclei.

Although the nanoparticles entered the cells, the chances of nanoparticles directly contacting DNA strands may have been limited. To thoroughly expose DNAs to the nanoparticles, whole genomic DNA strands were first isolated and then incubated with the nanoparticles for 48 and 72 h. The DNA samples were resolved by agarose gel electrophoresis. Any damaged DNA strands would migrate into the gel more quickly than the intact DNA. The results showed that the negative control and the nanoparticle-treated DNA were at the starting point, while a significantly faster DNA migration was observed in the positive control (*EcoRI* enzyme-treated DNA) (Figure 4c,d). These results again suggested that the nanoparticles do not cause obvious DNA damage within 72 h. The above data are consistent with our early observations that the nanoparticles do not penetrate and internalize into the nucleus.

DNA Repair Enzyme Activity. To assess DNA damage from a different angle, an indirect measurement was employed. The measurement was based on the cell stress response induced by DNA damage. When DNA is damaged, a corresponding repair pathway in the cell will be activated, resulting in increased enzymatic activity related to DNA repair (*30*). The detection of DNA repair proteins and their level of enzymatic activity reflect the extent of the DNA damage (*26*). oxo-dG is a common mutated DNA that plays a major role in mutagenesis and carcinogenesis (*26*). Several repair proteins including hOgg1 and APE-1/ref-1 are needed to correct oxo-dG (*28*). The hOggl activity was tested using a substrate DNA containing an oxo-dG lesion at the 9th position. The hOgg1, as an initiation enzyme for the BER repair pathway, can cleave the substrate from 23 to 9 bp fragments. This feature signals the specific enzymatic activity of hOgg1. Figure 5a,b shows the 9 bp DNA fragment appearing in the positive control but not in sample cells and the negative control, indicating that the hOgg1 enzymatic activity was only slightly increased in cells exposed to the nanoparticles than that of the untreated sample. The normalized activity in the sample with 0.5 mg/mL nanoparticles treatment was increased to 1.57 as compared to the activity of the negative control, which was set as 1 (Figure 5c).

Usually, more than one DNA repair enzyme may be activated in an oxidative stress. To test the validity of the hOggl activity result, the APE-1 enzymatic activity was determined (Figure 5d). The substrate DNA (20 bp) contained a tetrahydrofuran

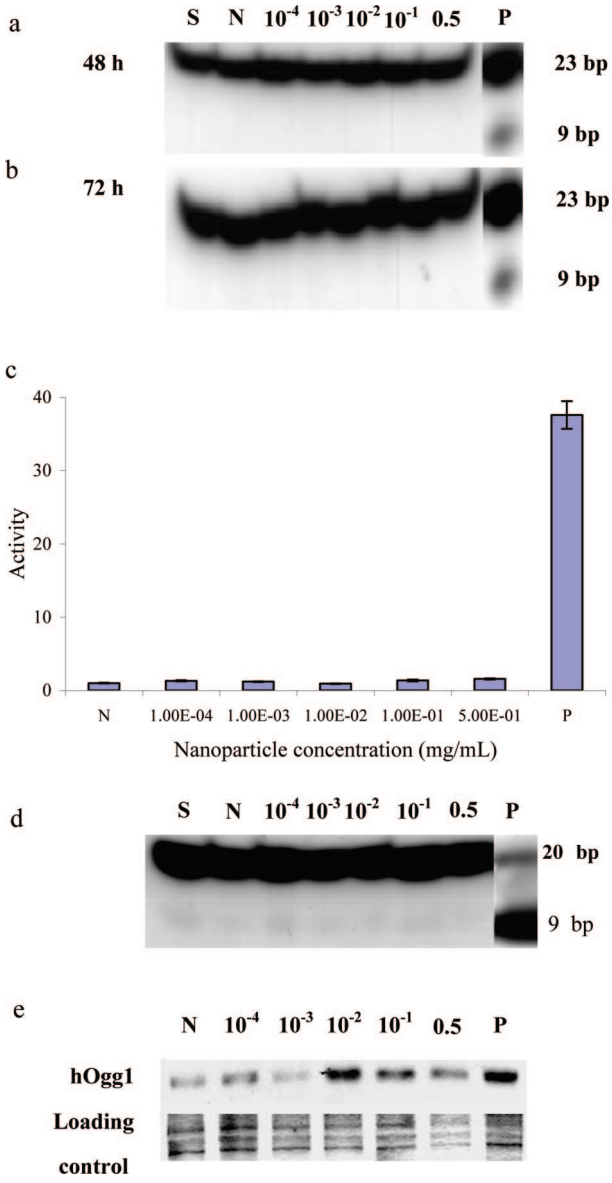

Figure 5. Analysis of the nanoparticle effects on the DNA repair enzymatic activity (concentration unit, mg/mL). (a and b) hOgg1 enzymatic activity assay. The samples were treated with the nanoparticles at indicated concentrations. The positive control was induced by Cd^{2+} treatment at 1 mM for 4 h; N, negative control (PBS only). (c) hOgg1 activities after 72 h of incubation with the nanoparticles. (d) APE-1 activity. The samples were incubated with nanoparticles for 72 h, and the enzymatic activity was examined. (e) hOgg1 expression in A549 cells detected by Western blotting within 72 h of incubation. The positive control was induced by Cd^{2+} treatment at 1 mM for 4 h. The gel was stained with Coomassie Blue to confirm equal sample loadings.

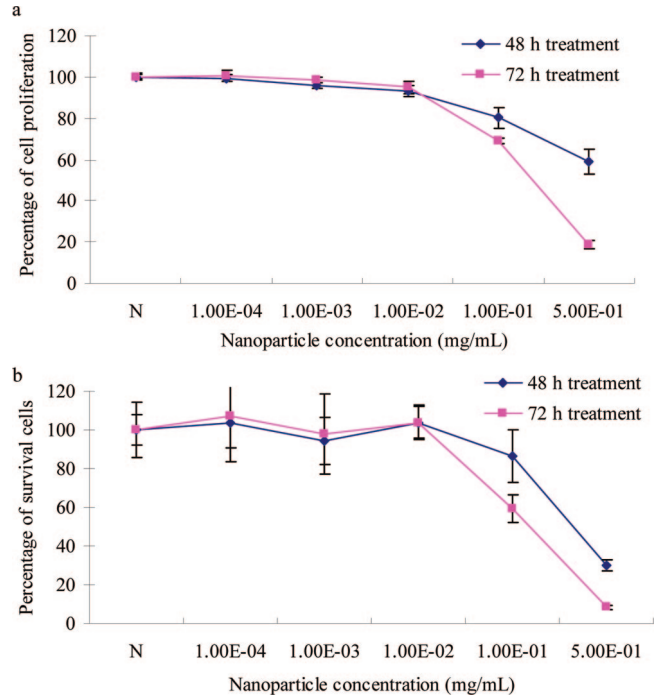

Figure 6. Cytotoxic effects of the nanoparticles. (a) Cytotoxicity on A549 cells after 48 and 72 h of incubation with the luminescent silica nanoparticles using the MTT assay. The percentage of survival cells was relative data as compared to the negative control cells. The data are presented with means ± SD. (b) Cytotoxicity on A549 cells after 48 and 72 h of incubation with the luminescent silica nanoparticles using Trypan Blue exclusion assay. The Trypan Blue exclusion assay directly determines the cell death. The data are presented with means ± SD.

synthetic apyrimidinic/apurinic site (THF-AP) that could be cleaved by APE-1 enzyme, resulting in a 9 bp DNA fragment. The resultant change was not significant based on Student's *t* test for the degraded 9 bp band, although the nanoparticle-treated cells showed slight induction of APE-1 activity than the control. It should be noted that the APE-1 activity is easily induced (*28*). Thus, the nanoparticles did not induce strong stress responses of DNA repair proteins by inflicting DNA damage in the cells.

Furthermore, the amount of the hOgg1 DNA repair protein was determined using Western blotting with a polyclonal antibody from Trevigen (Figure 5e). Surprisingly, the hOgg1 protein amount was significantly increased upon the incubation with nanoparticles for 72 h. It is difficult to explain this phenomenon, since most reports demonstrate that an increase in the amount of protein is directly related to its activity (*31*). However, increased protein levels may not directly indicate enhanced activity since interactions between DNA repair proteins and signaling proteins may hamper the activity assayed in clued extracts. Stoichiometry using His-Ogg1 is routinely performed in our laboratory, and this can truly reflect the DNA repair activity. Induction of DNA repair activity may vary with cell types and oxidative stresses (*32*). In this case, we speculate that the nanoparticles may induce hOgg1 expression through a pathway other than a common oxidation since no significant DNA damage is observed. It should also be noted that an increase in DNA repair proteins is a beneficial response to prevent severe DNA injury, which may contribute to reduced cell death rates (see below).

Cell Survival Rate after Nanoparticle Treatment. We then examined the nanoparticle toxicity at the cellular level using a cell proliferation assay [3-(4,5-dimethylthiazol-2-yl)-2,5-diphenyltetrazolium bromide (MTT) assay]. The living cells were able to convert the tetrazolium component of a compound into a formazan product that has absorption at 570 nm. The absorbance was proportional to the amount of living cells. The cell survival rates were determined against the negative control (Figure 6a). As the concentration of the nanoparticles increased, the cell survival rate decreased. A concentration of 0.1 mg/mL of nanoparticles caused a reduced but not significant rate (80%, 48 h; 69%, 72 h). However, at a high concentration of 0.5 mg/mL nanoparticles, the cell survival percentage was drastically reduced to 60 (48 h) and 18% (72 h) (50% of inhibition concentration, $IC_{50} = 0.25$ mg/mL for 72 h of treatment; Table 1). To verify this result, a Trypan Blue exclusion assay was performed.

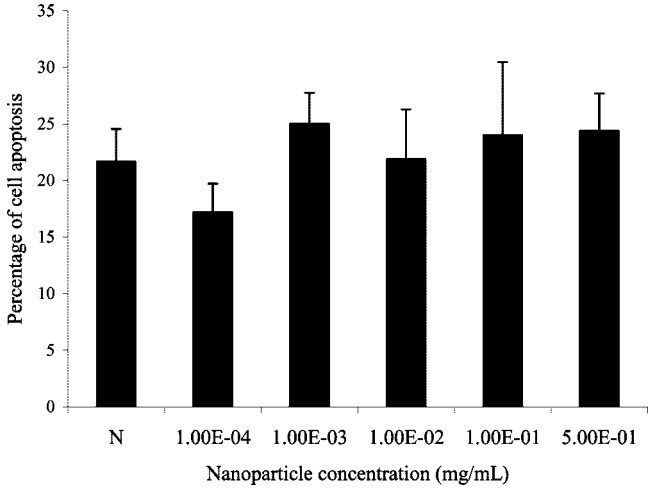

Figure 7. Vybrant assay for the detection of the luminescent silica nanoparticles on the cell apoptosis. A549 cells were treated with the nanoparticles at the indicated concentrations for 72 h and stained with the fluorescence dyes for 5 min. The data were derived from confocal fluorescence microscopy and the percentage of each type (apoptotic and necrotic) of cells was calculated against the total counts (at least 100 cells were counted in each sample). The data showed here are only apoptotic cells. The data are presented with means ± SD. All of the data are representative of three experiments.

Table 1. IC_{50} Values (mg/mL) of the Nanoparticle Cytotoxicity to Different Cells

incubation time (h)	A549 cell MTT assay	A549 cell Trypan Blue assay	alveolar macrophage cell MTT assay
48	<0.5	0.357	0.028
72	0.25	0.174	0.011

Our assumption was that the nanoparticles at such a high concentration might attach to the cell surface and interfere with membrane function or metabolism despite having demonstrated no toxic effects in DNA damage assays. In the Trypan Blue exclusion assay, dead cells with leaky membranes are stained with Trypan Blue dye, while living cells exclude the blue dye and are not stained. The results showed that the nanoparticle concentration determined the cell survival rate (Figure 6b). As the nanoparticle concentration was below 0.01 mg/mL, the cell survival rate was close to 100%. However, as the concentration reached 0.1 mg/mL, the cell survival percentage was reduced to 86 (48 h) and 60% (72h). As the concentration increased to 0.5 mg/mL, only 30 (48 h) (IC_{50} = 0.357 mg/mL; Table 1) and 8% (72 h) (IC_{50} = 0.174 mg/mL) of the cells survived. Interestingly, we tested the toxic properties of the nanoparticles in the alveolar macrophage cell line MHS and results demonstrated a stronger toxicity to the MHS cells (IC_{50} = 0.028 at 48 h and IC_{50} = 0.011 at 72 h) than to A549 cells. This is consistent with previous reports that macrophages, as actively phagocytic cells, are prone to infectious pathogens or toxic molecules.

Study of Cell Apoptosis. The above two assays could only detect cell necrosis. To understand whether the nanoparticles could cause cell damage through apoptosis in cells, the Vybrant apoptosis assay was employed, in which apoptotic cells were probed by green YO-PRO-1 dye and the necrotic cells were stained by red dye propidium iodide. The percentage of apoptotic cells was determined by counting green-colored cells. The negative control showed 19.8 ± 4.4% of cell apoptosis (Figure 7). The sample cells presented apoptotic cell rates ranging from 17.2 ± 2.5 to 26.3 ± 3.5%. The results were comparable with the negative control including 0.5 mg/mL sample based on Student's *t* test ($P > 0.05$), indicating that the nanoparticles do not induce noticeable apoptosis, although cell necrosis occurred at the concentration of 0.5 mg/mL.

Conclusions

In summary, our results suggest that the dye-doped luminescent silica nanomaterials have low genotoxicity and cytotoxicity in A549 cells. One interesting discovery in this study is that the nanoparticles appear to induce higher hOgg1 expression than its enzymatic activity. This behavior is different from conventional toxicity results. We speculate that the nanoparticles may cause cells to initiate some antistress response through a specific pathway. Induction of DNA repair proteins appears to be a beneficial response to prevent severe DNA injury, which may explain the lowered cytotoxicity. The multiple studies of DNA toxicological properties suggest that the genotoxicity is less severe than the cellular damage. This may suggest that there are different toxicities among nanoparticles. It is possible that cell death can be caused by less genome damage but more cellular organelle destruction (*28*). Genotoxicity is associated with apoptosis that is initiated by complex regulation (interconnected signaling mechanisms) (*33, 34*), whereas cellular toxicity, such as necrosis in this study, may be directly caused by membrane lipid peroxidation, energy depletion, ROS production, and cytosolic organelle destruction (*28, 35*). However, despite being considered of low genotoxicity, accumulated silica may induce chronic or acute toxicity if one is exposed to high concentrations of silica over a long period of time (*29, 36, 37*). Thus, the long-term toxicity of the silica nanoparticles needs further investigation. In conclusion, the combination of low toxicity and high luminescence of dye-doped silica nanoparticles provides a promising luminescent labeling reagent for future biomedical applications.

Acknowledgment. We thank Ms. Donna Laturnus, Dr. Michael Atkinson, and Dr. Edward Carlson at the Basic Sciences Imaging Center at the UND School of Medicine and Health Sciences for their help on fluorescence and electron microscopy imaging. We thank Dr. David Peirce, Dr. Harmon Abrahamson, and Dr. Thomas Ballintine in the Chemistry Department at UND for their proofreading of this manuscript. The work was partially supported by the American Heart Association Scientist Development Grant 535010N, NIH ES14690, the National Science Foundation Grant CHE-0616878, UND Faculty Seed Money Awards, and Society of Analytical Chemists of Pittsburgh Start Award.

References

(1) Zhao, X., Hilliard, L. R., Wang, K., and Tan, W. (2004) Bioconjugated silica nanoparticles for bioanalysis. In *Encyclopedia of Nanoscience and Nanotechnology* (Nalwa, H. S., Ed.) pp 255–268, American Scientific Publishers, Stevenson Ranch.

(2) Medintz, I. L., Trammell, S. A., Mattoussi, H., and Mauro, J. M. (2004) Reversible modulation of quantum dot photoluminescence using a protein-bound photochromic fluorescence resonance energy transfer acceptor. *J. Am. Chem. Soc. 126*, 30–31.

(3) Chan, W. C. W., and Nie, S. M. (1998) Quantum dot bioconjugates for ultrasensitive nonisotopic detection. *Science 281*, 2016–2018.

(4) Lin, Z., Su, X., Mu, Y., and Jin, Q. (2004) Methods for labeling quantum dots to biomolecules. *J. Nanosci. Nanotechnol. 4*, 641–645.

(5) Han, M., Gao, X., Su, J. Z., and Nie, S. M. (2001) Quantum-dot-tagged microbeads for multiplexed optical coding of biomolecules. *Nat. Biotechnol. 19*, 631–635.

(6) Koo, Y. E., Cao, Y., Kopelman, R., Koo, S. M., Brasuel, M., and Philbert, M. A. (2004) Real-time measurements of dissolved oxygen inside live cells by organically modified silicate fluorescent nanosensors. *Anal. Chem. 76*, 2498–2505.

(7) Park, E. J., Brasuel, M., Behrend, C., Philbert, M. A., and Kopelman, R. (2003) Ratiometric optical PEBBLE nanosensors for real-time magnesium ion concentrations inside viable cells. *Anal. Chem. 75*, 3784–3791.
(8) Esch, M. B., Locascio, L. E., Tarlov, M. J., and Durst, R. A. (2001) Detection of viable Cryptosporidium parvum using DNA-modified liposomes in a microfluidic chip. *Anal. Chem. 73*, 2952–2958.
(9) Ho, J.-a. A., and Durst, R. A. (2000) Preparation of reagents for the determination of fumonisin B1 by flow-injection immunoanalysis. *Anal. Chim. Acta 414*, 51–60.
(10) Zhao, X., Tapec-Dytioco, R., and Tan, W. (2003) Ultrasensitive DNA detection using highly fluorescent bioconjugated nanoparticles. *J. Am. Chem. Soc. 125*, 11474–11475.
(11) Zhao, X., Bagwe, R. P., and Tan, W. (2004) Development of organic-dye-doped silica nanoparticles in a reverse microemulsion. *Adv. Mater. 16*, 173–176.
(12) Santra, S., Zhang, P., Wang, K., Tapec, R., and Tan, W. (2001) Conjugation of biomolecules with luminophore-doped silica nanoparticles for photostable biomarkers. *Anal. Chem. 73*, 4988–4993.
(13) Santra, S., Wang, K., Tapec, R., and Tan, W. (2001) Development of novel dye-doped silica nanoparticles for biomarker application. *J. Biomed. Opt. 6*, 160–166.
(14) Zhao, X., Hilliard, L. R., Mechery, S. J., Wang, Y., Bagwe, R. P., Jin, S., and Tan, W. (2004) A rapid bioassay for single bacterial cell quantitation using bioconjugated nanoparticles. *Proc. Natl. Acad. Sci. U.S.A. 101*, 15027–15032.
(15) Hoshino, A., Fujioka, K., Oku, T., Suga, M., Sasaki, Y. F., Ohta, T., Yasuhara, M., Suzuki, K., and Yamamoto, K. (2004) Physicochemical properties and cellular toxicity of nanocrystal quantum dots depend on their surface modification. *Nano Lett. 4*, 2163–2169.
(16) Kirchner, C., Liedl, T., Kudera, S., Pellegrino, T., Javier, A. M., Gaub, H. E., Stoelzle, S., Fertig, N., and Parak, W. J. (2005) Cytotoxicity of colloidal CdSe and CdSe/ZnS nanoparticles. *Nano Lett. 5*, 331–338.
(17) Shiohara, A., Hoshino, A., Hanaki, K., Suzuki, K., and Yamamoto, K. (2004) On the cyto-toxicity caused by quantum dots. *Microbiol. Immunol. 48*, 669–675.
(18) Derfus, A. M., Chan, W. C. W., and Bhatia, S. N. (2004) Probing the cytotoxicity of semiconductor quantum dots. *Nano Lett. 4*, 11–18.
(19) Lovrić, J., Bazzi, H. S., Cuie, Y., Fortin, G. R. A., Winnik, F. M., and Maysinger, D. (2005) Differences in subcellular distribution and toxicity of green and red emitting CdTe quantum dots. *J. Mol. Med. 83*, 377–385.
(20) Bagwe, R. P., Yang, C., Hilliard, L. R., and Tan, W. (2004) Optimization of dye-doped silica nanoparticles prepared using a reverse microemulsion method. *Langmuir 20*, 8336–8342.
(21) Kaneko, T., Saeki, K., Lee, T., and Mizuno, N. (1996) Improved retrograde axonal transport and subsequent visualization of tetramethylrhodamine (TMR)-dextran amine by means of an acidic injection vehicle and antibodies against TMR. *J. Neurosci. Methods* 157–165.
(22) Gharaee-Kermani, M., Ullenbruch, M., and Phan, S. H. (2005) Animal models of pulmonary fibrosis. *Methods Mol. Med. 117*, 251–259.
(23) Rosi, N. L., and Mirkin, C. A. (2005) Nanostructures in biodiagnostics. *Chem. Rev. 105*, 1547–1562.
(24) Elia, M. C., Storer, R. D., McKelvey, T. W., Kraynak, A. R., Barnum, J. E., Harmon, L. S., DeLuca, J. G., and Nichols, W. W. (1994) Rapid DNA degradation in primary rat hepatocytes treated with diverse cytotoxic chemicals: Analysis by pulsed field gel electrophoresis and implications for alkaline elution assays. *Environ. Mol. Mutagen. 24*, 181–191.
(25) Wu, M., Stockley, P. G., and Martin, W. J. (2002) An improved western blotting technique effectively reduces background. *Electrophoresis 23*, 2373–2376.
(26) Kannan, S., Pang, H., Foster, D. C., Rao, Z., and Wu, M. (2006) Human 8-oxoguanine DNA glycosylase increases resistance to hyperoxic cytotoxicity in lung epithelial cells and involvement with altered MAPK activity. *Cell Death Differ. 13*, 311–323.
(27) Cooke, M. S., Evans, M. D., Dizdaroglu, M., and Lunec, J. (2003) Oxidative DNA damage: Mechanisms, mutation, and disease. *FASEB J. 17*, 1195–1214.
(28) Wu, M. (2005) DNA repair proteins as molecular therapeutics for oxidative and alkylating lung injury. *Curr. Gene Ther. 5*, 225–236.
(29) Wu, M., He, Y. H., Kobune, M., Xu, Y., Kelley, M. R., and Martin, W. J. n. (2002) Protection of human lung cells against hyperoxia using the DNA base excision repair genes hOgg1 and Fpg. *Am. J. Respir. Crit. Care Med. 166*, 192–199.
(30) Cortina, M. S., Gordon, W. C., Lukiw, W. J., and Bazan, N. G. (2005) Oxidative stress-induced retinal damage up-regulates DNA polymerase gamma and 8-oxoguanine-DNA-glycosylase in photoreceptor synaptic mitochondria. *Exp. Eye Res. 81*, 742–750.
(31) Pines, A., Perrone, L., Bivi, N., Romanello, M., Damante, G., Gulisano, M., Kelley, M. R., Quadrifoglio, F., and Tell, G. (2005) Activation of APE1/Ref-1 is dependent on reactive oxygen species generated after purinergic receptor stimulation by ATP. *Nucleic Acids Res. 33*, 4379–4394.
(32) Wu, M., Kelley, M. R., Hansen, W. K., and Martin, W. J. n. (2001) Reduction of BCNU toxicity to lung cells by high-level expression of O(6)-methylguanine-DNA methyltransferase. *Am. J. Physiol. Lung Cell Mol. Physiol. 280*, 755–761.
(33) Bonde, C., Noraberg, J., Noer, H., and Zimmer, J. (2005) Ionotropic glutamate receptors and glutamate transporters are involved in necrotic neuronal cell death induced by oxygen-glucose deprivation of hippocampal slice cultures. *Neuroscience 136*, 779–794.
(34) Kostrzewa, R. M. (2000) Review of apoptosis vs. necrosis of substantia nigra pars compacta in Parkinson's disease. *Neurotoxicol. Res. 2*, 239–250.
(35) Pearl-Yafe, M., Kaminitz, A., Yolcu, E. S., Yaniv, I., Stein, J., and Askenasy, N. (2007) Pancreatic islets under attack: Cellular and molecular effectors. *Curr. Pharm. Des. 13*, 749–760.
(36) Watterson, A., Gorman, T., Malcolm, C., Robinson, M., and Beck, M. (2006) The economic costs of health service treatments for asbestos-related mesothelioma deaths. *Ann. N. Y. Acad. Sci. 1076*, 871–881.
(37) Lin, W., Huang, Y. W., Zhou, X. D., and Ma, Y. (2006) In vitro toxicity of silica nanoparticles in human lung cancer cells. *Toxicol. Appl. Pharmacol. 217*, 252–259.
(38) Wisniowski, P. E., Spech, R. W., Wu, M., Doyle, N. A., Pasula, R., and Martin, W. J., II (2000) Vitronectin protects alveolar macrophages from silica toxicity. *Am. J. Respir. Crit. Care. Med. 162*, 733–739.

TX7001959